Detection of sodium absorption in WASP-17b with Magellan*

G. Zhou† and D. D. R. Bayliss

Research School of Astronomy and Astrophysics, Australian National University, Cotter Road, Weston Creek, ACT 2611, Australia

ABSTRACT

We present the detection of sodium absorption in the atmosphere of the extrasolar planet WASP-17b, an inflated 'hot Jupiter' in a tight orbit around an F6 dwarf. In-transit observations of WASP-17 made with the Magellan Inamori Kyocera Echelle (MIKE) spectrograph on the 6.5-m Magellan Telescope were analysed for excess planetary atmospheric absorption in the Na I 'D' doublet spectral region. Using the interstellar sodium absorption lines as reference, we detect a 0.58 ± 0.13 per cent transit signal, with 4.5σ confidence, at 1.5 Å bandwidth around the stellar sodium absorption feature. This result is consistent with the previous Very Large Telescope detection of sodium in WASP-17b, confirming that the planet has a highly inflated atmosphere.

Key words: methods: observational – techniques: spectroscopic – planets and satellites: atmospheres – planets and satellites: individual: WASP-17b – stars: individual: WASP-17 – planetary systems.

1 INTRODUCTION

Numerous techniques have now been developed to study the atmospheric properties of transiting planets. For example, emission from the planet inferred by observations of the secondary eclipse can reveal their day-side temperatures (e.g. Charbonneau et al. 2005; Deming et al. 2005). Additional infrared photometry of the phase variation can map the temperature distribution of 'hot Jupiter' planets (Knutson et al. 2007). As light from the host star passes through the upper atmosphere of a planet during the primary transit, it is possible to investigate the planetary atmospheric composition via transmission spectroscopy. Charbonneau et al. (2002) employed this technique to detect the atmosphere of an extrasolar planet for the first time. Their observations of HD 209458b with the *Hubble Space Telescope* (*HST*) revealed a 0.02 per cent transit signal in the Na I resonance lines, indicative of Na I absorption in the upper atmosphere of the planet.

The amount of absorption measured by transmission spectroscopy probes the wavelength dependence of the height of the planet's atmosphere. The optical depth is dependent on the temperature, surface gravity and composition of the atmosphere. For 'hot Jupiters', the opacity is predicted to be strongest at the Na I and K I resonance lines in the optical, whilst molecular species such as water and methane dominate the near-infrared part of the spectrum (Seager & Sasselov 2000; Brown 2001; Hubbard et al. 2001). In recent years, the use of transmission spectroscopy has led to a series of discoveries in the study of 'hot Jupiter' atmospheres, including the escaping atomic hydrogen envelope around HD 209458 (Vidal-Madjar et al. 2003) and the presence of haze in HD 189733b (Pont et al. 2008).

Despite the recent successes, the expected planetary absorption signal is very small, and the technique of transmission spectroscopy remains difficult. So far, Na I detection via ground-based high-resolution spectroscopy has only been achieved on three transiting planets, HD 209458b (Snellen et al. 2008; Langland-Shula et al. 2009; Jensen et al. 2011), HD 189733b (Redfield et al. 2008) and WASP-17b (Wood et al. 2011), along with numerous unsuccessful attempts (e.g. Narita et al. 2005; Bozorgnia et al. 2006). Recent detections around the K I resonance line by narrow-band photometry have also been achieved with XO-2b (Sing et al. 2011) and HD 80606b (Colón et al. 2012). High-resolution spectroscopic detections often require 8–10 m class telescopes, with data taken in optimal conditions, yielding signal-to-noise ratio (S/N) values $\gg 100$ pixel^{-1}. Even so, the transit signal is heavily contaminated by much larger systematic trends, such as echelle blaze function variations (Winn et al. 2004), CCD non-linearity (Snellen et al. 2008) and telluric contamination (e.g. Albrecht et al. 2009; Langland-Shula et al. 2009; Jensen et al. 2011). Here, we present a novel approach of using the nearby interstellar absorption lines to correct for the majority of these systematic effects.

WASP-17b (Anderson et al. 2010) is a 0.49 $M_{\rm Jup}$, 1.99 $R_{\rm Jup}$ planet in a retrograde, 3.7 d orbit (Bayliss et al. 2010; Triaud et al. 2010). The equilibrium temperature of the planet, measured by *Spitzer* photometry of the secondary eclipse, is 1771 ± 35 K, assuming zero albedo and full redistribution (Anderson et al. 2011). Recent observations by Wood et al. (2011) with GIRAFFE on the Very Large Telescope detected a 1.46 per cent transit in the Na I 'D' lines at 0.75 Å bandwidth, a level 10 times larger than detections made around any other planet.

Bayliss et al. (2010) obtained time series spectra of WASP-17 during the primary transit event to measure the spin–orbit alignment of the system. In this study, we present an analysis of these data to monitor for Na I absorption in the planetary atmosphere.

---

*This paper includes data gathered with the 6.5 metre Magellan Telescopes located at Las Campanas Observatory, Chile.

†E-mail: george@mso.anu.edu.au
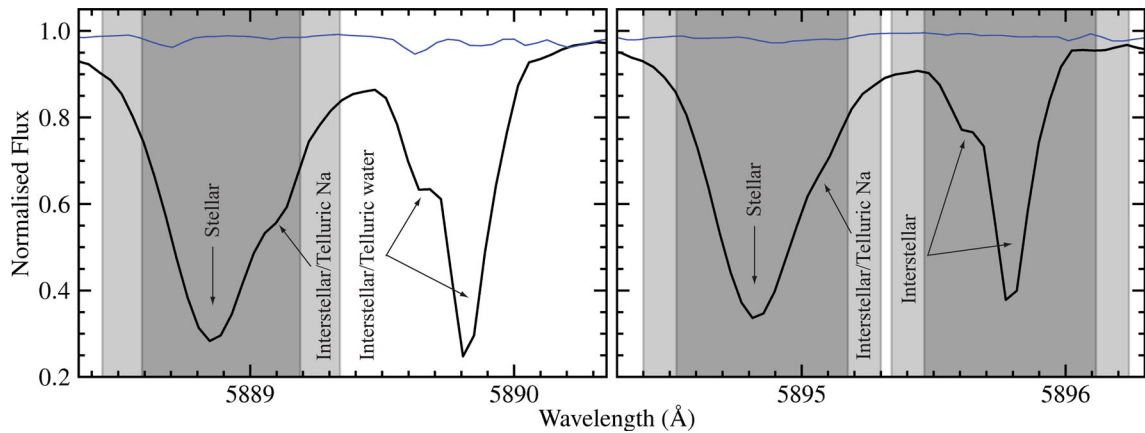
Figure 1. Plotted are the Na I 'D' doublet regions of the template spectrum, with D_1 on the left-hand panel, D_2 on the right-hand panel, as observed with Magellan. The broad stellar absorption features are resolved from the narrower interstellar components. Each line is also blended with additional interstellar and telluric Na I components (Wood et al. 2011). The minimum and maximum half-bandwidths of 0.60 and 0.90 Å are filled in grey. The telluric absorption spectrum, as observed with a rapidly rotating B star, is overplotted in blue.

2 OBSERVATIONS AND DATA ANALYSIS

Observations of WASP-17 were obtained with the Magellan Inamori Kyocera Echelle (MIKE) spectrograph on the 6.5-m Magellan II (Clay) telescope, located at Las Campanas Observatory, on the night of 2010 May 11. The spectra were obtained at a resolution of $\lambda/\Delta\lambda \approx 48\,000$ in the wavelength range 5000–9500 Å, over echelle orders 37–69. Each exposure was 600 s in length, giving an average S/N of 82 pixel^{-1} over the Na I 'D' doublet region, within the echelle order of 58. Th–Ar arc lamp exposures were taken bracketing each exposure. Of the 37 object exposures, 21 were taken out-of-transit, 11 in-transit, two during ingress and three during egress. Two observations were rejected for having S/N < 60 – one was taken during egress, the other whilst out-of-transit near the end of the night, at high airmass. Observations were paused for 30 min, whilst the planet was in-transit, due to the zenith limit of the telescope. The details of the observations and data reduction are given in Bayliss et al. (2010).

2.1 Spectral analysis

2.1.1 Correction of systematic trends

A wavelength shift of $\sim 1\,\mathrm{km\,s^{-1}}$ was registered over the night, due to a combination of instrument drift, airmass change, system orbital dynamics and the Rossiter–McLaughlin (RM) effect (McLaughlin 1924; Rossiter 1924). The average shift per exposure was calculated by weighted averaging over all orders not contaminated by telluric absorption, and corrected for with the IRAF[1] package RV. We found time- and wavelength-dependent variations in the blaze function between exposures, and corrected for this using the method described in Winn et al. (2004). We fitted the residual difference between an observed spectrum and an averaged template with an order 5 smoothed B-spline. In order to avoid removing the actual transit signal in the analysis, we corrected the spectrum of order n with the averaged residual fits of orders $n - 1$ and $n + 1$. Finally, a template spectrum was created by a 2σ clipped averaging of all blaze corrected object spectra. The Na I 'D' doublet region of the template spectrum is shown in Fig. 1.

2.1.2 Subtraction of telluric features

Telluric absorption lines originating from water and Na are dispersed unevenly within the stellar and interstellar Na I features (Fig. 1). Nightly variations in the strength of these telluric lines can overwhelm the planetary Na I absorption signal, and must be removed in the spectral analysis process. Some transmission spectroscopy observations (e.g. Winn et al. 2004; Narita et al. 2005; Redfield et al. 2008) removed their telluric contamination by subtracting a smooth B star spectrum; others (e.g. Snellen et al. 2008; Wood et al. 2011) performed the same subtraction using synthetic telluric spectra. We obtained a telluric template spectrum by averaging two observations of the B star HD 129116. For each WASP-17 observation, the telluric spectrum, scaled and shifted by fitting for the telluric water dominated regions around the Na I 'D' doublet, was divided from the object spectrum. We note that the telluric scaling deviates from the airmass function at the start of the night, indicative of variations in the atmospheric water content. The telluric scaling correlates well with airmass for the second half of the night. We see no significant telluric Na lines in the telluric spectrum, and assume that any telluric Na variations scale with water. Similarly, Snellen et al. (2008) pointed out that although telluric Na varies seasonally, it correlates well with water and oxygen over a single night.

2.1.3 Flux extraction

Following equation (1) of Snellen et al. (2008), we integrated the flux within a half-bandwidth of the line centroid, corrected against two adjacent reference continuum regions. We found that the blaze and reference continuum region corrections could not remove all systematic effects, but variations in the interstellar Na I lines correlate strongly with that of the stellar Na I lines. The strong interstellar Na I absorption doublet can be found 1 Å ($\sim 50\,\mathrm{km\,s^{-1}}$) redwards of their stellar components (Fig. 1). We can assume that the strength of the interstellar absorption features are invariant with time, as we do not expect the interstellar medium to be changing on the time-scale of hours. The proximity of the interstellar to the stellar features makes them excellent references to correct for any additional, higher order systematic variations. We hence extract the flux of both the stellar and interstellar absorption lines in our analysis.

The Na I flux was calculated as the ratio between the sum of the contributing fluxes from each component of the doublet and that of the same regions in the template spectrum. The line centroids of the stellar Na I 'D' doublet are located at 5888.89 (D_1) and 5894.85 Å (D_2). The adjacent interstellar components are located at 5889.82 and 5895.80 Å.

We find that the interstellar D_1 line is severely contaminated by telluric water lines (Fig. 1). The line shows large time-dependent variations, most likely due to the incomplete subtraction of telluric lines blended within the stellar absorption feature. The relative level of telluric contamination can be quantified by taking the sum equivalent width of the telluric lines within the stellar and interstellar regions; for the stellar D_1 and D_2 lines, the sum telluric equivalent widths are 0.0046 and 0.0043 Å, and for the interstellar D_1 and D_2 lines, the sum telluric equivalent widths are 0.0092 and 0.0008 Å. The interstellar D_1 line contains more than twice the amount of telluric contamination as the stellar D_1, D_2 and the interstellar D_2 lines. We therefore do not use the interstellar D_1 line in our subsequent analyses.

For each exposure, we performed a Gaussian centroid fit to each line to remove any uncorrected wavelength shifts, and then summed the flux around the fitted centroid position. The reference continuum regions to the left and right of the line centroid, for the stellar Na I D_1 line, are centred at 5887 and 5893 Å, respectively, and for the stellar and interstellar Na I D_2 lines at 5893 and 5897 Å, respectively. These reference regions are not located directly adjacent to the stellar lines to avoid overlapping with the interstellar components.

The use of the nearby interstellar Na I absorption lines as reference is facilitated by the large velocity difference between WASP-17 and the sight line interstellar medium. The heliocentric mean velocity of WASP-17 is $-49.5\,\mathrm{km\,s^{-1}}$ (Anderson et al. 2010), whilst we measure the sight line interstellar medium velocity to be $-0.5\,\mathrm{km\,s^{-1}}$, consistent with the velocity of the local interstellar cloud (e.g. Redfield & Linsky 2008). The separation between the stellar and interstellar Na I absorption features is ~1 Å in wavelength space. To investigate the minimum stellar–interstellar feature separation required for this technique, we simulate a stellar–interstellar absorption pair with two equal-height Gaussians of full widths at half maximum 0.4 and 0.2 Å. Various separations between the two Gaussians are tested, and the flux is extracted about the broader stellar Gaussian at 0.6 Å bandwidth. We find that at separations less than 0.54 Å, the influence of the interstellar line on the extracted stellar line flux becomes greater than our measurement error of 0.15 per cent, corresponding to a minimum velocity separation requirement of $27.5\,\mathrm{km\,s^{-1}}$ between the target and the sight line interstellar medium.

For a single exposure, the Na I flux, F_{rel}, relative to the ratio between the stellar fluxes $F_{\mathrm{D1,stellar}}$, $F_{\mathrm{D2,stellar}}$ and the interstellar flux $F_{\mathrm{D2,interstellar}}$, is

$$F_{\mathrm{rel}} = \frac{w_1 F_{\mathrm{D1,stellar}} + w_2 F_{\mathrm{D2,stellar}}}{F_{\mathrm{D2,interstellar}}} . \tag{1}$$

The weights w_1 and w_2 are inversely proportional to the scatter of the light curves calculated for each stellar line individually, according to

$$F_{\mathrm{D1,rel}} = \frac{F_{\mathrm{D1,stellar}}}{F_{\mathrm{D2,interstellar}}} \tag{2}$$

and

$$F_{\mathrm{D2,rel}} = \frac{F_{\mathrm{D2,stellar}}}{F_{\mathrm{D2,interstellar}}} . \tag{3}$$

The flux of each individual component is calculated by their counts relative to the same regions in the template spectrum, corrected by the counts in the reference continuum regions. For example, the flux in the stellar D_1 line is derived from the counts in the object spectrum about the absorption line and reference region, O_{D1} and O_{ref}, and the counts in the same regions in the template spectrum, T_{D1} and T_{ref}, by

$$F_{\mathrm{D1,stellar}} = \frac{O_{\mathrm{D1}}/O_{\mathrm{ref}}}{T_{\mathrm{D1}}/T_{\mathrm{ref}}} . \tag{4}$$

The error in the relative flux is derived from the average S/N within the bandwidth, divided by the square root of the number of spectral points included in the bandwidth.

2.1.4 Modelling of in-transit line profile variations

The strength of the absorption signal is strongly dependent on the bandwidth within which the flux is summed; the relationship between the bandwidth and transit depth provides information on the properties of the planetary atmosphere. One limitation with our methodology of using the interstellar Na I lines as calibrators is that we must restrict the size of the bandwidth used. To avoid overlapping between the stellar and interstellar Na I components, the maximum half-bandwidth we employ is 0.90 Å. The minimum half-bandwidth of 0.60 Å is determined by the in-transit line profile variations that result from the distortions induced by the RM effect.

The observed line profile is a convolution between the intrinsic stellar absorption profile, a time-varying rotational kernel that takes into account the occulted stellar disc and the instrument response kernel. To model the distortions, the intrinsic Na I stellar absorption profile was approximated using a high-resolution solar spectrum (Delbouille, Roland & Neven 1990). Solar rotational broadening is four times less than that of WASP-17, whilst the instrumental broadening in the solar template is 100 times less than our observations. Hirano et al. (2010) provided a Gaussian approximation to the analytical solution of the rotation kernel. Using theoretical V-band limb darkening coefficients from Claret & Bloemen (2011), with Anderson et al. (2011) stellar parameters for WASP-17, we calculated a Gaussian rotational kernel with a standard deviation of 0.12 Å. The kernel is modified at each time step to reflect the position of the planet over the stellar disc during transit. We modelled the MIKE instrument kernel with a Gaussian of 0.052 Å standard deviation, matching a spectral resolution of $\lambda/\Delta\lambda = 48\,000$ at 5890 Å. The solar template is convolved at each time step, and the flux around the absorption line is summed and normalized against the out-of-transit flux.

The upper panel of Fig. 2 shows the resulting transit light curve derived from the flux around Na I D_1 at various bandwidths. The distortions to the transit light curve, calculated as the absolute difference from the 2.0 Å bandwidth light curve, become larger than our measurement error of 0.15 per cent at bandwidths narrower than 0.60 Å (Fig. 2, lower panel).

We therefore extracted the flux around the Na I 'D' doublet at seven half-bandwidths, from 0.60 to 0.90 Å, evenly spaced at 0.05 Å intervals. As an example, the 0.75 Å half-bandwidth light curve is plotted in Fig. 3, and the fluxes are set out in Table 1.

2.2 Light curve analysis

The transit depth, D, is the ratio of the average out-of-transit flux to the average in-transit flux, F_{OOT} and F_{INT}, respectively
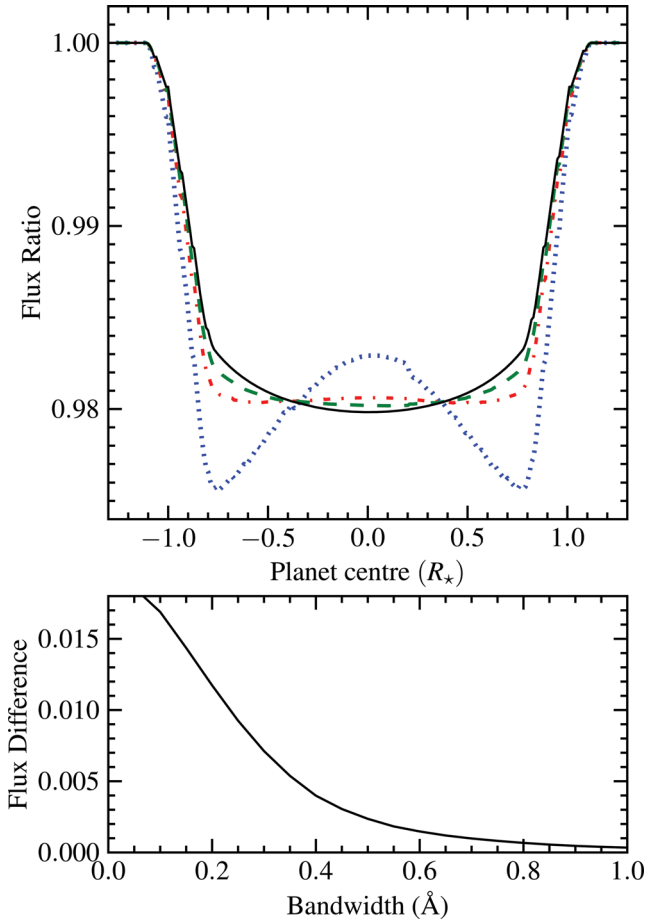
Figure 2. The top panel plots the model transit light curves from fluxes extracted around the Na I D$_1$ line at bandwidths of 2.0 Å (black solid line), 0.7 Å (green dashed line), 0.5 Å (red dot–dashed line) and 0.3 Å (blue dotted line). The bottom panel shows the absolute flux difference for the narrow bandwidths light curves, relative to a 2.0 Å bandwidth light curve.
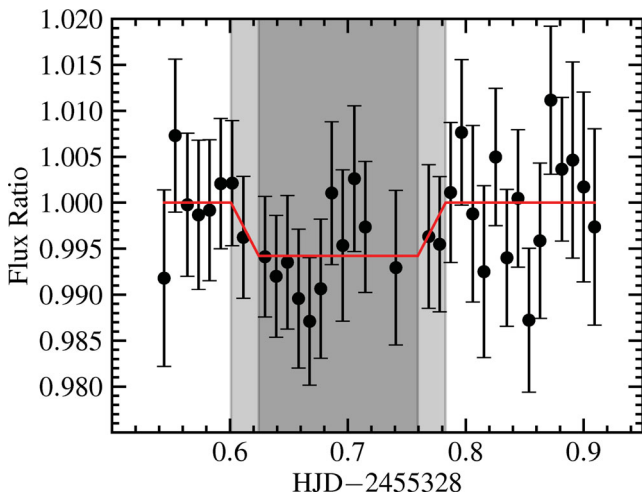
Figure 3. An example light curve, extracted around the stellar Na I D$_1$ and D$_2$ lines at 0.75 Å half-bandwidth, is plotted. The red line plots the 0.58 ± 0.13 per cent transit depth fit. The darker shade marks the in-transit proportion of the light curve, whilst the lighter shade marks ingress and egress.

Table 1. Fluxes for the 0.75 Å half-bandwidth light curve.

HJD − 245 5328	F_{rel}	ΔF_{rel}	Comment
0.544	0.9918	0.0096	Out-of-transit
0.554	1.0073	0.0083	Out-of-transit
0.564	0.9998	0.0078	Out-of-transit
0.573	0.9987	0.0081	Out-of-transit
0.583	0.9992	0.0077	Out-of-transit
0.592	1.0021	0.0071	Out-of-transit
0.602	1.0021	0.0068	Ingress
0.611	0.9962	0.0066	Ingress
0.630	0.9941	0.0066	In-transit
0.639	0.9920	0.0066	In-transit
0.649	0.9935	0.0073	In-transit
0.658	0.9896	0.0076	In-transit
0.668	0.9871	0.0069	In-transit
0.677	0.9906	0.0076	In-transit
0.686	1.0011	0.0078	In-transit
0.696	0.9954	0.0082	In-transit
0.706	1.0026	0.0079	In-transit
0.715	0.9974	0.0071	In-transit
0.741	0.9929	0.0084	In-transit
0.769	0.9963	0.0078	Egress
0.778	0.9955	0.0074	Egress
0.787	1.0011	0.0076	Out-of-transit
0.796	1.0077	0.0079	Out-of-transit
0.806	0.9988	0.0096	Out-of-transit
0.815	0.9925	0.0093	Out-of-transit
0.825	1.0050	0.0075	Out-of-transit
0.835	0.9940	0.0074	Out-of-transit
0.844	1.0005	0.0075	Out-of-transit
0.854	0.9872	0.0078	Out-of-transit
0.863	0.9959	0.0084	Out-of-transit
0.872	1.0112	0.0081	Out-of-transit
0.881	1.0036	0.0078	Out-of-transit
0.891	1.0046	0.0107	Out-of-transit
0.900	1.0017	0.0103	Out-of-transit
0.909	0.9974	0.0107	Out-of-transit

(Brown 2001):

$$D = 1 - \frac{F_{INT}}{F_{OOT}} . \tag{5}$$

Exposures with mid-times set during ingress or egress are excluded. Overall, there were 20 out-of-transit points and 11 in-transit points included in the calculations. The error in the transit depth, ΔD, is estimated from the standard deviation of the points in-transit and out-of-transit, σ_{INT} and σ_{OOT}, respectively:

$$\left(\frac{\Delta D}{1-D}\right)^2 = \left(\frac{\sigma_{INT}/\sqrt{N_{INT}}}{F_{INT}}\right)^2 + \left(\frac{\sigma_{OOT}/\sqrt{N_{OOT}}}{F_{OOT}}\right)^2 , \tag{6}$$

where N_{INT} and N_{OOT} are the number of points averaged in-transit and out-of-transit. The same analysis was performed at every bandwidth, the results of which are presented in Table 2. At 1.5 Å bandwidth, we detect a transit depth of 0.58 ± 0.13 per cent with 4.5σ confidence. We also performed the same light curve analysis on the fluxes extracted around the stellar Na I D$_1$ and D$_2$ lines individually, according to equations (2) and (3). The transit depths at 1.5 Å bandwidth for the D$_1$ and D$_2$ stellar lines are 0.53 ± 0.16 and 0.66 ± 0.10 per cent, respectively. The transit depths derived from each individual Na I line is consistent with each other and with that derived from the weighted average light curve.

Table 2. The transit depths at various bandwidths.

Bandwidth (Å)	Transit depth (per cent)
1.2	0.60 ± 0.14
1.3	0.60 ± 0.13
1.4	0.59 ± 0.13
1.5	0.58 ± 0.13
1.6	0.56 ± 0.13
1.7	0.50 ± 0.12
1.8	0.42 ± 0.11

3 DISCUSSION

Our Magellan transmission spectroscopic measurements detected a 0.58 per cent transit, at 4.5σ confidence, in the Na I 'D' doublet region of WASP-17, which is consistent with the results of Wood et al. (2011). This study confirms that WASP-17b shows the strongest Na I absorption signal measured to date. Given the low surface gravity and high equilibrium temperature of the planet, WASP-17b has the largest atmospheric scale height of all known transiting planets, facilitating the large transmission spectroscopic signal.

Interestingly, an extension of our analysis to narrower bandwidths could not replicate the steep increase in absorption strength as observed by Wood et al. (2011). It is unclear how the RM effect distortions to the absorption line profile were dealt with in this previous study, given that fluxes extracted at 0.375 Å half-bandwidth would have been severely affected. In addition, our results hint at a steep decrease in absorption strength for our broader bandwidths. This feature is potentially similar to the steep decrease observed by Wood et al. (2011) at 3.0 Å bandwidth, which was attributed primarily to the presence of clouds in the upper planetary atmosphere.

We can make a comparison between observations of HD 209458b and WASP-17b by scaling the former according to the differences in temperature and gravity between the two planets. The transit depth is governed by the atmospheric scale height of the planet and the radius ratio between the planet (R_P) and the host star ($R_\star$) (Brown 2001):

$$D = \frac{2\pi R_P(kT/\mu g)}{\pi R_\star^2}, \tag{7}$$

where T is the temperature, μ is the mean molecular weight of the atmosphere and g is the surface gravity of the planet. Such scaling assumes that the atmospheric structure is consistent between the planets, and the change in contribution from secondary effects is negligible, accounting only for the difference in temperature and bulk density between the two planets. Taking a scale height for HD 209458b of 500 km and μ of H_2, we multiply the Snellen et al. (2008) measurements by a factor of 2.4; the resulting estimates are plotted in Fig. 4. Our WASP-17b measurements match the scaled HD 209458b atmosphere remarkably well.

Similarly, the transit depths derived and scaled from models of Brown (2001) by Wood et al. (2011) are also plotted. The model prediction lies well above our measured signal. All transmission spectroscopy of transiting planets to date have consistently shown that the Na I signal is weaker than that of a cloudless model in local thermodynamic equilibrium. The close-in orbits of these 'hot Jupiters' mean that their atmospheres are highly irradiated, causing depletion of Na to form Na^+. Photoionization occurs in the upper levels of the atmosphere, whilst the line wings are formed in the denser lower atmosphere. The result of neutral Na depletion is therefore a reduction in the depth of the line cores (e.g. Barman et al.
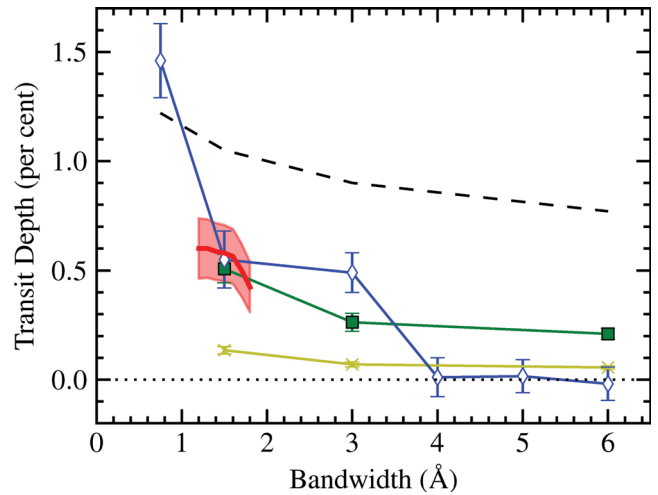
Figure 4. Plotted are the various observed and modelled Na I transit depths. The Magellan detection presented in this paper is shown by red shaded region. Blue diamonds plot the results of Wood et al. (2011). Green squares plot HD 209458b measurements from Snellen et al. (2008) after scaling by the WASP-17b scale height. Yellow crosses plot the original Snellen et al. (2008) measurements of HD 209458b. The Brown (2001) model prediction, as calculated and scaled by Wood et al. (2011), is plotted as the dashed line.

2002; Fortney et al. 2003). The presence of silicate and iron condensates in the upper atmosphere (Sudarsky, Burrows & Pinto 2000; Fortney et al. 2003; Sudarsky, Burrows & Hubeny 2003), combined with the slanted geometry inherent to transmission spectroscopy (Fortney 2005), also act to decrease the absorption signal.

We note that this study presents a ground-based spectroscopic Na I detection with the smallest telescope to date, in an S/N regime significantly lower than previous observations. This shows that the use of interstellar absorption features as reference is a robust technique that removes the majority of systematic effects. Langland-Shula et al. (2009) noted that better telluric subtractions could be achieved by taking interleaved smooth spectrum star observations, reducing the reliance on scaling a single telluric template to fit the observed spectrum. WASP-17 is by far the faintest target pursued by the transmission spectroscopy technique, and the positive detection opens up the possibility to explore other similarly inflated targets.

REFERENCES

Albrecht S., Snellen I., de Mooij E., Le Poole R., 2009, in Pont F., Sasselov D., Holman M., eds, Proc. IAU Symp. 253, Transiting Planets. Cambridge Univ. Press, Cambridge, p. 520
Anderson D. R. et al., 2010, ApJ, 709, 159
Anderson D. R. et al., 2011, MNRAS, 416, 2108

Barman T. S., Hauschildt P. H., Schweitzer A., Stancil P. C., Baron E., Allard F., 2002, ApJ, 569, L51

Bayliss D. D. R., Winn J. N., Mardling R. A., Sackett P. D., 2010, ApJ, 722, L224

Bozorgnia N., Fortney J. J., McCarthy C., Fischer D. A., Marcy G. W., 2006, PASP, 118, 1249

Brown T. M., 2001, ApJ, 553, 1006

Charbonneau D., Brown T. M., Noyes R. W., Gilliland R. L., 2002, ApJ, 568, 377

Charbonneau D. et al., 2005, ApJ, 626, 523

Claret A., Bloemen S., 2011, A&A, 529, A75

Colón K. D., Ford E. B., Redfield S., Fortney J. J., Shabram M., Deeg H. J., Mahadevan S., 2012, MNRAS, 419, 2233

Delbouille L., Roland G., Neven L., 1990, Atlas Photometrique DU Spectre Solaire de [lambda] 3000 a [lambda] 10000. Universite de Liege, Liege

Deming D., Seager S., Richardson L. J., Harrington J., 2005, Nat, 434, 740

Fortney J. J., 2005, MNRAS, 364, 649

Fortney J. J., Sudarsky D., Hubeny I., Cooper C. S., Hubbard W. B., Burrows A., Lunine J. I., 2003, ApJ, 589, 615

Hirano T., Suto Y., Taruya A., Narita N., Sato B., Johnson J. A., Winn J. N., 2010, ApJ, 709, 458

Hubbard W. B., Fortney J. J., Lunine J. I., Burrows A., Sudarsky D., Pinto P., 2001, ApJ, 560, 413

Jensen A. G., Redfield S., Endl M., Cochran W. D., Koesterke L., Barman T. S., 2011, ApJ, 743, 203

Knutson H. A. et al., 2007, Nat, 447, 183

Langland-Shula L. E., Vogt S. S., Charbonneau D., Butler P., Marcy G., 2009, ApJ, 696, 1355

McLaughlin D. B., 1924, ApJ, 60, 22

Narita N. et al., 2005, PASJ, 57, 471

Pont F., Knutson H., Gilliland R. L., Moutou C., Charbonneau D., 2008, MNRAS, 385, 109

Redfield S., Linsky J. L., 2008, ApJ, 673, 283

Redfield S., Endl M., Cochran W. D., Koesterke L., 2008, ApJ, 673, L87

Rossiter R. A., 1924, ApJ, 60, 15

Seager S., Sasselov D. D., 2000, ApJ, 537, 916

Sing D. K. et al., 2011, A&A, 527, A73

Snellen I. A. G., Albrecht S., de Mooij E. J. W., Le Poole R. S., 2008, A&A, 487, 357

Sudarsky D., Burrows A., Pinto P., 2000, ApJ, 538, 885

Sudarsky D., Burrows A., Hubeny I., 2003, ApJ, 588, 1121

Triaud A. H. M. J. et al., 2010, A&A, 524, A25

Vidal-Madjar A., Lecavelier des Etangs A., Désert J.-M., Ballester G. E., Ferlet R., Hébrard G., Mayor M., 2003, Nat, 422, 143

Winn J. N., Suto Y., Turner E. L., Narita N., Frye B. L., Aoki W., Sato B., Yamada T., 2004, PASJ, 56, 655

Wood P. L., Maxted P. F. L., Smalley B., Iro N., 2011, MNRAS, 412, 2376

This paper has been typeset from a TEX/LATEX file prepared by the author.